

A Potential Vorticity Tendency Diagnostic Approach for Tropical Cyclone Motion*

LIGUANG WU AND BIN WANG

Department of Meteorology, School of Ocean and Earth Science and Technology, University of Hawaii at Manoa, Honolulu, Hawaii

(Manuscript received 3 May 1999, in final form 18 August 1999)

ABSTRACT

In order to understand the roles of various physical processes in baroclinic tropical cyclone (TC) motion and the vertical coupling between the upper- and lower-level circulations, a new dynamical framework is advanced. A TC is treated as a positive potential vorticity (PV) anomaly from environmental flows, and its motion is linked to the positive PV tendency. It is shown that a baroclinic TC moves to the region where the azimuthal wavenumber one component of the PV tendency reaches a maximum, but does not necessarily follow the ventilation flow (the asymmetric flow over the TC center). The contributions of individual physical processes to TC motion are equivalent to their contributions to the wavenumber one PV component of the PV tendency. A PV tendency diagnostic approach is described based on this framework. This approach is evaluated with idealized numerical experiments using a realistic hurricane model. The approach is capable of estimating TC propagation with a suitable accuracy and determining fractional contributions of individual physical processes (horizontal and vertical advection, diabatic heating, and friction) to motion. Since the impact of the ventilation flow is also included as a part of the influence of horizontal PV advection, this dynamical framework is more general and particularly useful in understanding the physical mechanisms of baroclinic and diabatic TC motion.

1. Introduction

Vortex motion is usually expressed in terms of the trajectory of a vortex center. This is essentially a quasi-Lagrangian approach. However, fundamental physical principles governing atmospheric motion are expressed in the Eulerian frame of reference. Therefore, in order to understand the mechanisms for TC motion, it is necessary to link the vortex motion with the atmospheric circulation (the TC circulation and its environment).

Tropical cyclones can displace westward and poleward relative to the steering flow at a speed of 1–3 m s⁻¹ (e.g., Carr and Elsberry 1990). This component of TC translation was termed propagation by Holland (1983). In the previous studies, TC translation is related to axially asymmetric flows over the TC center (the ventilation flow). The beta drift is an example of vortex propagation caused by the beta effect. Fiorino and Elsberry (1989) found that the beta drift in a barotropic model has almost the same speed as the uniform axially

asymmetric flow over the vortex center between a pair of counterrotating asymmetric gyres (the beta gyres). This finding has been confirmed by numerical experiments with barotropic models (e.g., Willoughby 1990, 1992; Peng and Williams 1990). The resulting asymmetric flow over the vortex center is referred to as the ventilation flow by Fiorino and Elsberry (1989). The propagation is found to be intimately linked to the orientation and strength of the beta gyres. Therefore, a key to understanding the barotropic beta drift is how the beta gyres are affected by various physical processes. For example, the development and maintenance of beta gyres have been extensively investigated with barotropic models in the presence of environmental flows (DeMaria 1985; Ulrich and Smith 1991; Smith 1991; Williams and Chan 1994; Li and Wang 1996; Wang et al. 1997). Li and Wang (1994) and Wang and Li (1995) demonstrated that the development and maintenance of beta gyres can also be understood from energetics considerations. For a detailed review, readers can refer to Wang et al. (1998).

Recently, the concept of the ventilation flow has been further extended to the baroclinic case and widely used in numerical simulations and PV diagnostics to understand baroclinic TC motion. It was suggested that the baroclinic beta drift velocity of an adiabatic baroclinic vortex is approximately equal to the geostrophic flow implied by asymmetric pressure gradients at the surface vortex center (Wang and Li 1992). By defining TC mo-

* School of Ocean and Earth Science and Technology Publication Number 5043 and IPRC Number IPRC-41.

Corresponding author address: Dr. Bin Wang, Department of Meteorology, University of Hawaii at Manoa, 2525 Correa Road, Honolulu, HI 96822.
E-mail: bwang@soest.hawaii.edu

tion as the movement of the middle-layer vortex, Shapiro (1992) argued that the TC translation in his three-layer model arises from the flow between the asymmetric gyres. In a tilted three-dimensional vortex capped with upper-level negative PV anomalies, Wu and Emanuel (1993) proposed that the upper-level negative PV anomalies (anticyclonic circulation) could affect low-level vortex motion through the so-called asymmetric penetration flows associated with the upper-level PV anomaly. In an adiabatic model, Wang and Holland (1996a) contend that the vortex movement is determined by both the asymmetric flow over the vortex core associated with beta gyres and the flow associated with vertical projection of tilted PV anomalies at upper levels. In the presence of diabatic heating, the diabatic heating can affect TC motion through the downward penetration flows associated with the anticyclonic PV anomalies aloft, which are continuously generated by diabatic heating, and through asymmetric divergent flows associated with convective asymmetries within the vortex core region (Wang and Holland 1996b). Although the asymmetric flows that arise from different mechanisms have been proposed, their relative contributions to TC motion have not been quantitatively assessed.

Both observational (Wu and Emanuel 1995a,b; Bender 1997) and modeling (Wang and Holland 1996a–c) studies indicate that there exist significant vertical variations in the asymmetric flow over the TC core region, while the TC moves as an entity. In this light, it is difficult to apply the concept of the ventilation flow to baroclinic TC motion and to explain the vertical coupling within the TC. Therefore, we need to look at the baroclinic TC motion in a different perspective. In particular, we will focus on understanding the contributions of various physical processes to baroclinic TC movement at each vertical level and the vertical coupling mechanism within a baroclinic TC.

An effort was recently made using a PV inversion approach to evaluate the influence of PV anomalies at various vertical levels on TC motion. The basic idea of this approach is to solve the inverse problem to obtain corresponding wind and mass fields for a given isolated PV anomaly (Hoskins et al. 1985; Davis 1992). Wu and Emanuel (1995a,b), Wu and Kurihara (1996), Shapiro (1996), and Shapiro and Franklin (1999) evaluated the contributions to TC motion from the individual PV anomalies associated with various parts of the TC and environmental flows. They found that the upper-level PV anomalies can play an important role in determining hurricane motion. The PV inversion method requires specifying a reference state (Hoskins et al. 1985). For instance, Wu and Emanuel used either a constant static stability (Wu and Emanuel 1993) or a climatological mean state (Wu and Emanuel 1995a,b). Since the penetration depth depends critically on the static stability (Hoskins et al. 1985; Shapiro and Montgomery 1993), the results can be considerably influenced by the assumptions made in the PV inversion.

TABLE 1. Summary of the numerical experiments.

Expt	Plane	Environmental flow (m s ⁻¹)	Heating
E1	f	-4	Adiabatic
E2	f	0	Diabatic
E3	beta	0	Adiabatic
E4	beta	0	Diabatic

In order to improve our understanding of the effects of various physical processes on baroclinic TC motion and the vertical coupling within a baroclinic TC, we describe in this paper a general dynamical framework for diagnosing baroclinic TC motion. Based on this framework, a new diagnostic approach is advanced, which can quantitatively identify the contributions of various physical processes to TC motion, including the influence of the ventilation flow. The dynamical framework for TC motion is described in section 2. The procedure of the new diagnostic approach is presented in section 3. The performance of the proposed approach is evaluated through idealized numerical experiments in section 4, followed by its application (section 5) and a brief summary (section 6).

2. A dynamic framework for baroclinic TC motion

Shapiro and Franklin (1995) documented the PV structure of Hurricane Gloria of 1985 with nested objective wind analyses of Omega dropwindsonde and airborne Doppler radar data. They showed that a TC is a strong localized positive PV anomaly in the lower and middle troposphere, and has a complex PV pattern in the upper outflow layer. Similar complex PV distributions in the upper outflow layer have been obtained from a variety of baroclinic hurricane models (Shapiro 1992; Wang and Holland 1996b; Wu and Kurihara 1996). In this study, the data used for diagnostics are derived from the output of a hurricane model, which is described in appendix A. Four numerical experiments are designed in this study. Table 1 summarizes the primary features of those experiments.

In σ coordinates, the definition of PV has the form of (see appendix B)

$$P = \left(-\frac{g}{p_s} \right) \left[(f + \zeta) \frac{\partial \theta}{\partial \sigma} + \frac{\partial u}{\partial \sigma} \frac{\partial \theta}{\partial y} - \frac{\partial v}{\partial \sigma} \frac{\partial \theta}{\partial x} \right], \quad (1)$$

where P represents PV; $(f + \zeta)$ and θ are, respectively, the vertical components of absolute vorticity and the potential temperature; u and v are, respectively, the zonal and meridional wind components; p_s is the surface pressure; and g is the gravitational acceleration.

Figure 1 shows the vertical PV distribution simulated in a resting environment on a beta plane (E4). The TC can be identified as a strong positive PV anomaly from the surface all the way to level 5 (about 300 mb). Clearly, the symmetric structure is well maintained in the

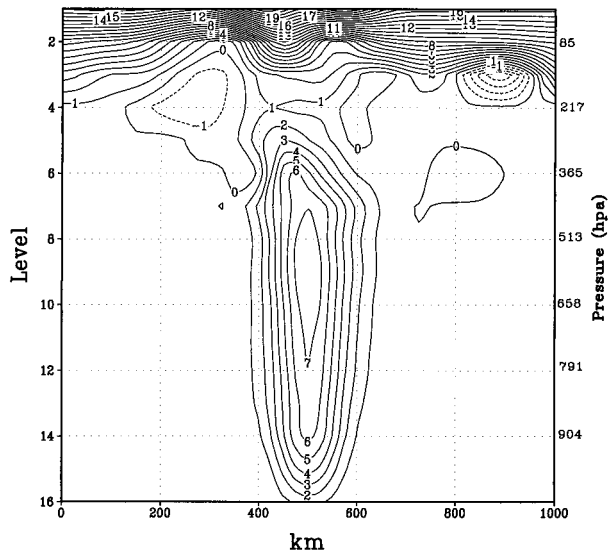


FIG. 1. The east–west (from right to left) cross section of PV at 48 h in E4. The contour intervals are 1 PVU.

middle and lower levels, while the PV anomaly tilts westward above 400 mb. In agreement with the previous observational and numerical studies, the positive PV with high values is confined within a radius of about 100 km. Above about 400 mb, there are regions of negative PV that are found to the west of the vortex core and approximately 400 km east of the vortex core. Wu and Kurihara (1996) pointed out that the condensational heating causes vertical redistribution of PV by creating negative PV anomalies in the upper levels and positive PV anomalies in the lower levels. The negative PV anomalies generated by diabatic heating are also advected by the upper-level outflow and environmental flow.

It has been shown that a TC can be treated as a three-dimensional positive PV anomaly, which is primarily confined in the middle and lower levels. As a result, the TC motion is actually equivalent to the movement of the localized positive PV anomaly. Therefore, an analysis of the movement of the PV anomaly can determine the corresponding TC motion. Based on PV thinking, Hoskins et al. (1985) illustrated that the ridges and troughs of a Rossby wave pattern tend to move to the regions with minimum and maximum PV tendencies, respectively, if the wave intensity does not change during the displacement. Similarly, TC motion can be directly related to the PV tendency.

We therefore focus on the PV tendency in the moving coordinates with a TC. In a moving reference frame, the PV tendency results from the local PV tendency observed in a fixed reference frame and the PV advection associated with the TC motion. It can be written as

$$\left(\frac{\partial P}{\partial t}\right)_m = \left(\frac{\partial P}{\partial t}\right)_f + \mathbf{C} \cdot \nabla P, \quad (2)$$

where the subscripts m and f indicate, respectively, the moving and fixed reference frames and \mathbf{C} is the velocity of TC motion, which is a function of height. Now we consider a vortex as a symmetric PV anomaly. The vortex motion is only related to the wavenumber one component of the PV tendency. Therefore, we will focus on the wavenumber one component of the PV tendency $[(\partial P/\partial t)_1]$. In the cylindrical coordinates moving with a TC center, the movement vector \mathbf{C} consists only of wavenumber one component (Wang et al. 1997). Thus we can write Eq. (2) in terms of the wavenumber one component as follows:

$$\left(\frac{\partial P}{\partial t}\right)_{1m} = \left(\frac{\partial P}{\partial t}\right)_{1f} + \mathbf{C} \cdot \nabla P_s, \quad (3)$$

where P_s is the symmetric PV component of PV.

The term on the left-hand side of Eq. (3) is associated with the development of the wavenumber one PV component. Since the development of a TC causes primarily changes of the symmetric component of PV, this term is negligible and Eq. (3) is dominated by the two terms on the right-hand side in the middle and lower troposphere, where the symmetric circulation is dominant. Figure 2 compares these two terms computed in E4. In order to reduce short-time fluctuations, which can be strongly influenced by small-scale effects, a running mean in the time domain is applied in Fig. 2. The wavenumber one component of the PV tendency (the right panels of Fig. 2) in the fixed reference frame is well balanced by the advection of the symmetric PV component associated with TC motion (the left panels in Fig. 2). Thus, Eq. (3) can be rewritten as

$$-\mathbf{C} \cdot \nabla P_s = \left(\frac{\partial P}{\partial t}\right)_{1f}. \quad (4)$$

Equation (4) indicates that a TC that is dominated by the symmetric circulation tends to move to the region with the maximum azimuthal wavenumber one component of the PV tendency. A similar conclusion was obtained by Chan (1984). Based on an observational study, he found that a TC tends to move to the area of maximum positive vorticity tendency.

Equation (4) directly relates vortex motion to PV tendency. Figure 3 shows the relationship between vortex motion and the wavenumber one component of the PV tendency in E4. The motion vectors (\mathbf{C}) are calculated from the tracks of the vortex centers at different levels. The vortex centers are determined by the positions of maximum PV. Consistent with Eq. (4), Fig. 3 indicates that the vortex moves to the region with maximum wavenumber one component of the PV tendency.

As shown in appendix B, the wavenumber one component of the PV tendency on the right-hand side of Eq. (4) can be calculated from the PV tendency equation as

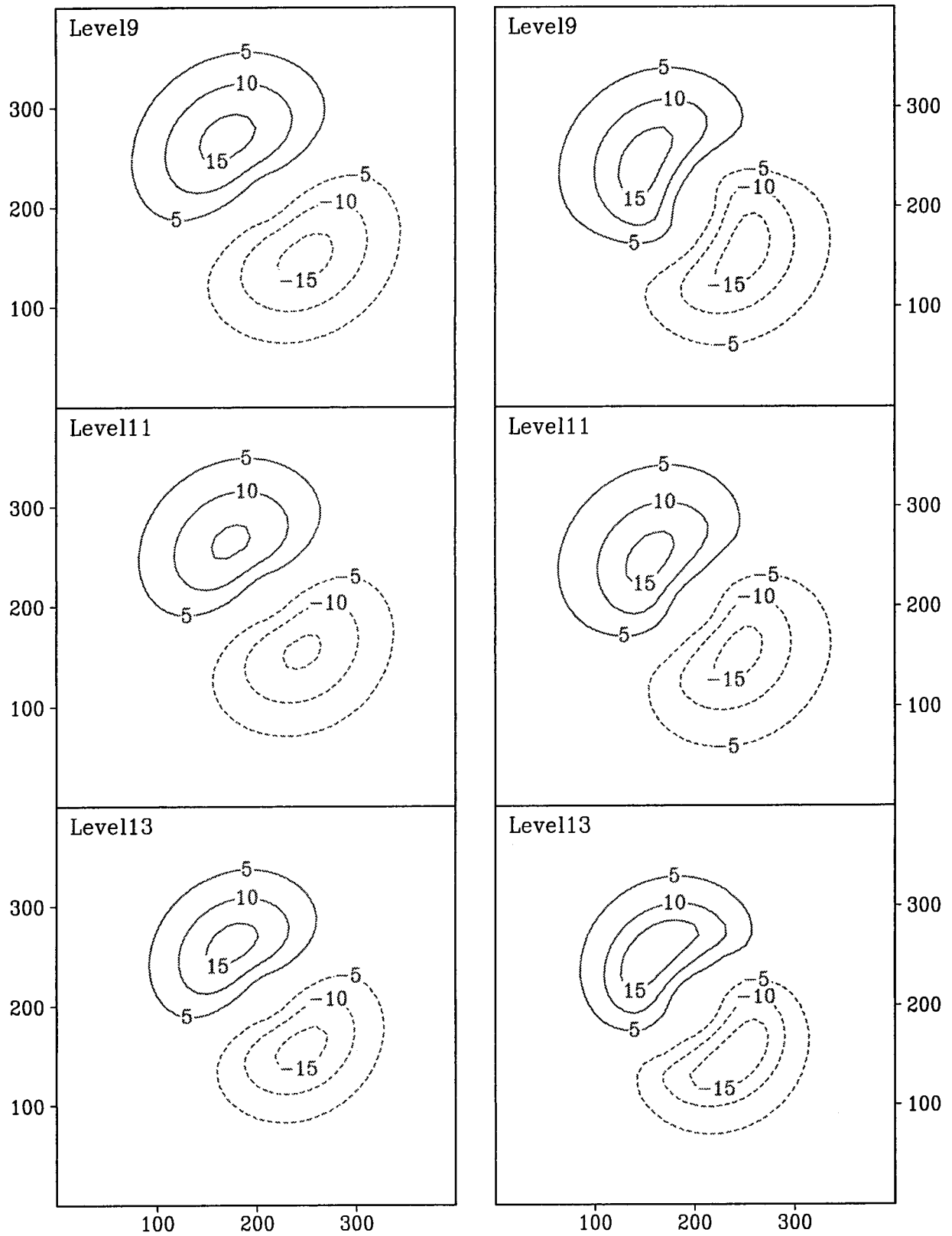
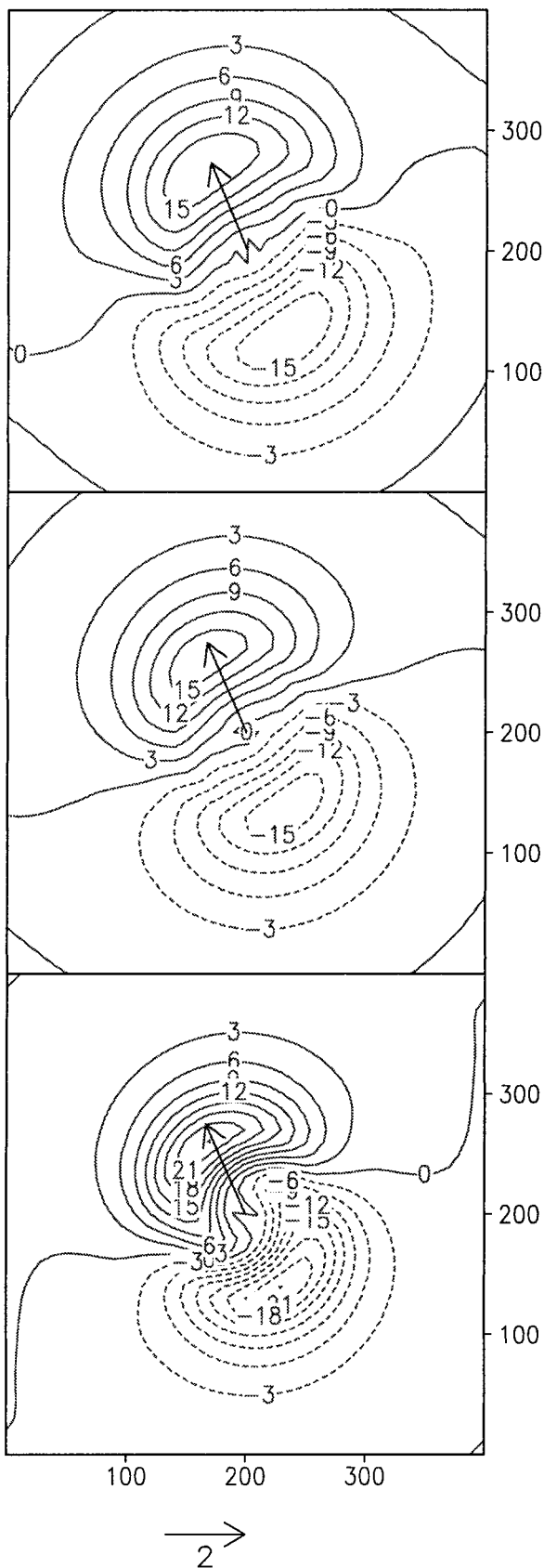


FIG. 2. The comparisons of PV tendency ($10^{-11} \text{ m}^2 \text{ s}^{-2} \text{ K kg}^{-1}$) associated with TC motion ($-\mathbf{C} \cdot \nabla P_s$) (left panels) with the wavenumber one component of the PV tendency (right panels) at 48 h in the diabatic experiment on a beta plane (E4).



$$\left(\frac{\partial P}{\partial t}\right)_1 = \Lambda_1 \left\{ -\mathbf{V} \cdot \nabla P - \dot{\sigma} \frac{\partial P}{\partial \sigma} - \frac{g}{p_s} \nabla_3 \cdot \left(-\frac{Q}{C_p \pi} \mathbf{q} + \nabla \theta \times \mathbf{F} \right) \right\}, \quad (5)$$

where $\dot{\sigma}$ is the vertical velocity in the σ coordinates, \mathbf{q} is the three-dimensional absolute vorticity vector, Λ_1 denotes an operator to obtain the wavenumber one component, ∇_3 is the three-dimensional gradient, and Q and \mathbf{F} denote diabatic heating rate and friction, respectively. Equation (5) suggests that the PV tendency results from horizontal and vertical PV advection, diabatic heating, and friction. With Eqs. (4) and (5), we can analyze the contributions of various physical processes by looking at how they contribute to the wavenumber one component of the PV tendency.

In general, all the physical processes on the right-hand side of Eq. (5) can affect TC motion. As mentioned in section 1, most previous studies only focus on the steering by the ventilation flow, which is included in the horizontal PV advection [the first term on the right-hand side of Eq. (5)]. In this sense, Eqs. (4) and (5) provide a general dynamical framework for the study of baroclinic TC motion.

3. The diagnostic approach

If we have observed data or the output from a hurricane model, the velocity of TC motion (\mathbf{C}) and the individual contributions of various terms in Eq. (5) can be estimated, provided the PV tendency and symmetric PV associated with the TC are computed. The computation procedures are as follows.

- 1) Calculate PV according to Eq. (1) and locate the vortex centers at given different levels.
- 2) Calculate PV tendencies associated with different terms in Eq. (5) and the total PV tendency.
- 3) Transform the quantities calculated in steps 1 and 2 to the cylindrical coordinates originating at on the vortex centers.
- 4) Obtain the axially symmetric PV component and the azimuthal wavenumber one component of the PV tendencies.
- 5) Transform the quantities calculated in step 4 back to the Cartesian coordinates.
- 6) Compute the gradient of P_s and apply Eq. (4) to each grid point (denoted by subscript i). This will result in a set of linear algebraic equations,

FIG. 3. The relationship between the total tendency of the wavenumber one PV component with contour intervals of $(3 \times 10^{-11} \text{ m}^2 \text{ s}^{-2} \text{ K kg}^{-1})$ and the TC motion vectors (the maximum is 2.4 m s^{-1}) at level 9 (top, 580 mb), 11 (middle, 730 mb), and 13 (bottom, 850 mb) at 60 h in the diabatic experiment on a beta plane (E4).

$$-c_x \left(\frac{\partial P_s}{\partial x} \right)_i - c_y \left(\frac{\partial P_s}{\partial y} \right)_i = \left(\frac{\partial P}{\partial t} \right)_{li}, \quad (6)$$

from which the zonal (c_x) and meridional (c_y) components of the velocity of the vortex motion at each level will be determined.

- 7) Considering a specified domain in the vicinity of the TC center, use the least square method to estimate c_x and c_y by minimizing (Press et al. 1986):

$$\sum_{i \leq N} \left[c_x \left(\frac{\partial P_s}{\partial x} \right)_i + c_y \left(\frac{\partial P_s}{\partial y} \right)_i + \left(\frac{\partial P}{\partial t} \right)_{li} \right]^2, \quad (7)$$

where N is the number of total grid points in the specified domain.

Notice that if $(\partial P/\partial t)_{li}$ is an individual contribution on the right-hand-side term of Eq. (5), the corresponding c_x and c_y denote the contributions of this term to the vortex motion. The performance and sensitivity of this PV diagnostic approach are addressed in the next section.

4. Evaluation of the diagnostic approach

The performance of the proposed PV tendency diagnostic approach is first evaluated by comparing the vortex speed estimated with the PV tendency procedures described in section 3 (hereafter the estimated speed) with the speed calculated from the 2-h difference of TC center locations (hereafter the Lagrangian speed). Since the least square method is used, the estimated speed may depend on the number of the total grid points (N) or the size of the specified domain. In order to examine the sensitivity of the estimated speed to the domain size, we compared the results derived from different domain sizes. It is found that the estimated speed is independent of the domain size if the domain is larger than $150 \times 150 \text{ km}^2$. This suggests that such large domains can provide sufficient information for accurately estimating the TC speed. This is because the PV anomaly is primarily confined in a radius of about 100 km (Fig. 1). We define a domain in all the following calculations as a square area of $300 \times 300 \text{ km}^2$.

Experiments E1 and E2 (Table 1) are first used to evaluate the performance of the diagnostic approach. Experiment E1 is a dry run on an f plane, in which the TC moves with the easterly environmental flow of 4 m s^{-1} . Figure 4 shows the comparison of the estimated speed with the Lagrangian speed at level 11 (730 mb) in this experiment. The zonal component of the estimated speed is slightly smaller than that of the Lagrangian speed. The difference is about 0.20 m s^{-1} . In the meridional direction, the two speeds are almost the same. Experiment E2 is a diabatic experiment on an f plane in a resting environment. In this case, no physical mechanism can make the TC move. Figure 5 is the same as Fig. 4 but for E2. As expected, the zonal and meridional components of the estimate speed are very close

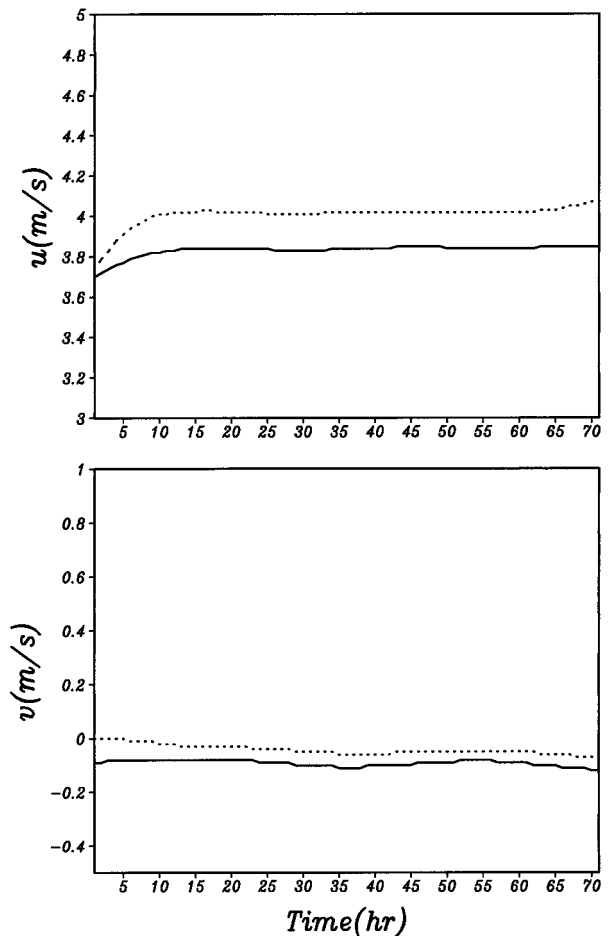


FIG. 4. Comparisons of the (top) zonal and (bottom) meridional velocities estimated with the 2-h difference of TC center positions (dashed) and with PV tendencies (solid) at level 11 (730 mb) in the adiabatic experiment on an f plane with an environmental flow of -4 m s^{-1} (E1).

to zero, except for very small fluctuations. As shown later, those fluctuations are due to the influence of diabatic heating.

Experiments E3 and E4 are further used to evaluate the PV diagnostic approach (Table 1). Both experiments are run on a beta plane in a resting environment, and the vortices move westward and poleward due to the interaction between the meridional gradient of the planetary vorticity and the primary vortex circulation. The TC motion in these two experiments has been referred to as the beta drift and recently investigated through numerical simulations (see section 1). In E3, the diabatic heating and the friction were turned off (the adiabatic case) while they were all retained in E4 (the diabatic heating case). Figure 6 shows the time series of the estimated beta-drift speed at level 11 (730 mb) in E3 compared with the Lagrangian speed. The components of the estimated speed in both zonal and meridional directions agree well with the Lagrangian speed at that level. In E4, although the accuracy is affected by the

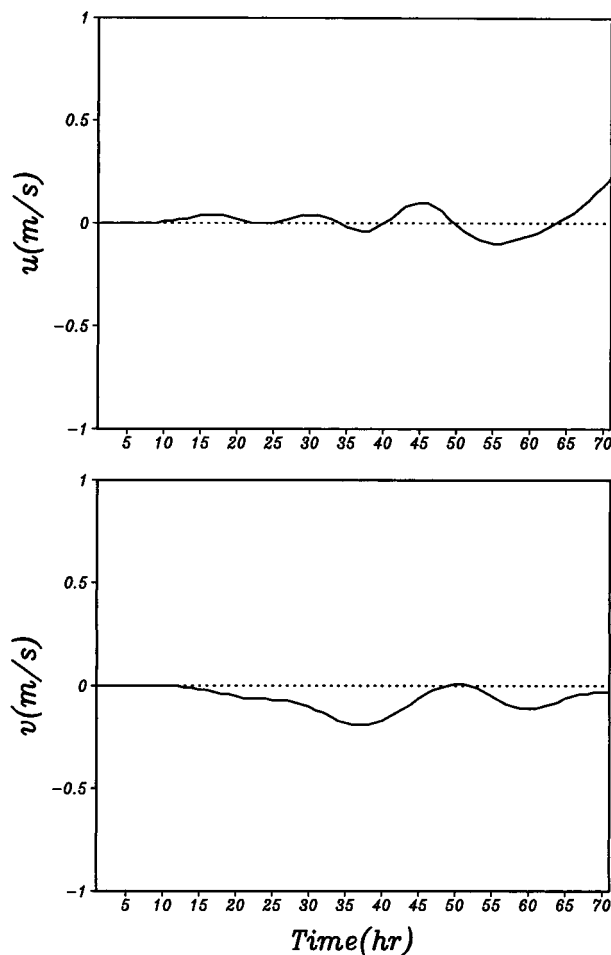


FIG. 5. Comparisons of the (top) zonal and (bottom) meridional velocities estimated with the 2-h difference of TC center positions (dashed) and with PV tendencies (solid) at level 11 (730 mb) in the diabatic experiment on an f plane in a resting environment (E2).

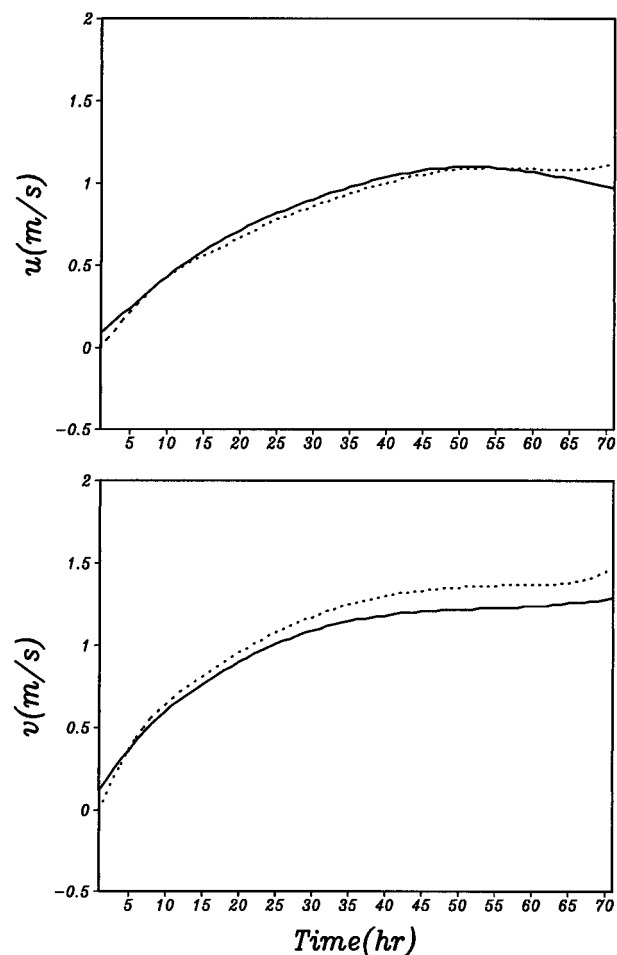


FIG. 6. Comparisons of the (top) zonal and (bottom) meridional velocities estimated with the 2-h difference of TC center positions (dashed) and with PV tendencies (solid) at level 11 (730 mb) in the adiabatic experiment on a beta plane in a resting environment (E3).

diabatic heating, the estimated speed remains good (Fig. 7). Therefore, it is suggested that the proposed diagnostic approach provides a reliable estimation of TC speed with an acceptable accuracy.

In the derivation of Eq. (4), we have assumed that the wavenumber one component of the PV component in the moving coordinates is negligibly small. This assumption may not hold in the upper troposphere because the cyclonic circulation decreases with height and significant asymmetric PV anomalies exist in the upper levels. To examine this possibility, we calculated the root-mean-square error (rmse) of the estimated speed at different levels. In E3 (Fig. 8), the rmse in the middle and lower troposphere is less than 0.1 m s^{-1} , whereas in the upper troposphere, it is between 0.1 and 0.22 m s^{-1} except at level 4 (220 mb), where the rmse's for the zonal and meridional components reach 0.39 and 0.55 m s^{-1} , respectively. The relative large errors are primarily due to the weak symmetric cyclonic PV over the center and strong asymmetric PV at the upper levels.

In the diabatic case (E4), the development of the asymmetric circulation in the upper levels results in large errors. Figure 9 shows the rmse for the diabatic experiment (E4). The rmse is large in the outflow layer compared with that in the middle levels. Meanwhile, it is also relatively large in the lowest model level. These large errors are due to the reduced intensity of the symmetric TC circulation and the enhanced asymmetric circulations owing to the diabatic heating and surface friction. In the boundary layer, the friction significantly reduces symmetric circulations, while the asymmetric surface fluxes enhance asymmetric circulations (Fig. 1). In the middle and lower levels (levels 8–15), where the cyclonic symmetric circulation dominates, the mean rmse is less than 0.27 m s^{-1} .

5. Determination of the contributions of various processes to TC motion

As mentioned in section 3, the proposed diagnostic approach is also useful to quantitatively identify the

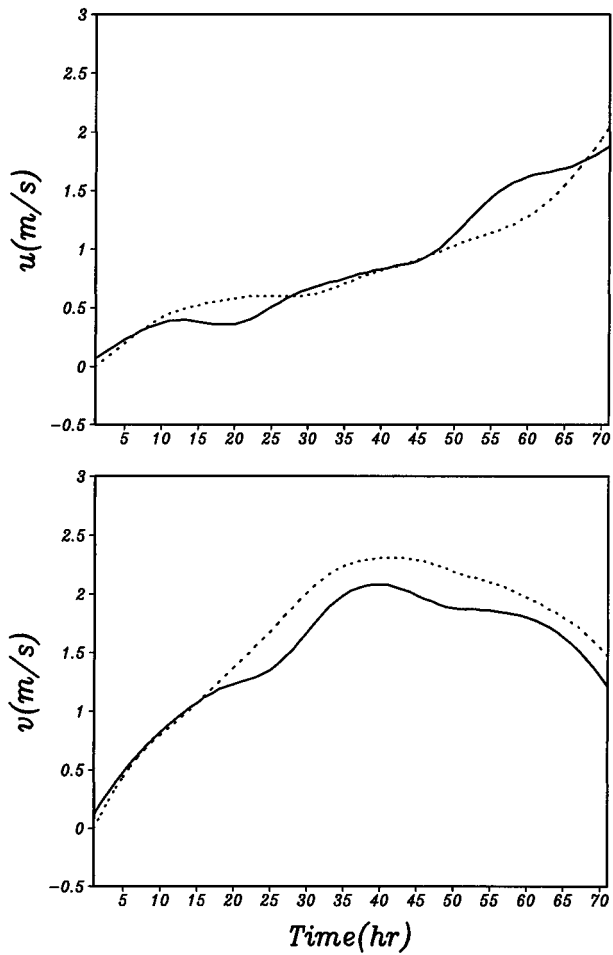


FIG. 7. Comparisons of the (top) zonal and (bottom) meridional velocities estimated with the 2-h difference of TC center positions (dashed) and with PV tendencies (solid) at level 11 (730 mb) in the diabatic experiment on a beta plane in a resting environment (E4).

fractional contributions of various physical processes indicated on the right-hand side of Eq. (5) to the vortex motion at a given level. To demonstrate this capability, we use the idealized experiments in Table 1, because the physical mechanisms for the TC motion in these experiments are well known. In E1, the vortex is advected by the uniform environmental flow. If the PV associated with a TC comprises primarily the symmetric and wavenumber one components, the horizontal advection includes not only the advection of symmetric PV by the asymmetric flow (steering), but also the advection of the wavenumber one PV component by the symmetric circulation. However, in E1, no physical mechanism can produce the axially asymmetric PV component. The horizontal advection can only arise from the horizontal PV advection by the environmental flow. This contribution is equal to the speed of the environmental flow. The environmental steering is well estimated with the proposed PV tendency diagnostic approach (figure not shown).

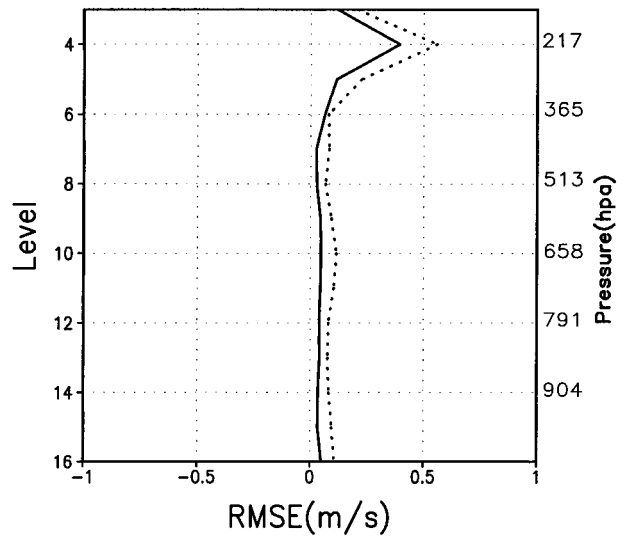


FIG. 8. The rmse of the estimated velocities in the diabatic experiment on a beta plane in a resting environment (E3). The solid and dashed lines are for zonal and meridional components, respectively.

In E2, although the diabatic heating and friction are included, no physical mechanism can produce asymmetries in the TC circulation. In other words, none of the physical processes have a contribution to the TC motion. Figure 10 shows the contributions of horizontal PV advection, vertical PV advection, diabatic heating, and friction. Except for very small fluctuations in the contribution of diabatic heating, as expected, all the physical processes have little influence on the vortex motion. Comparison of Figs. 5 and 10 reveals that the small fluctuations reflected in zonal and meridional ve-

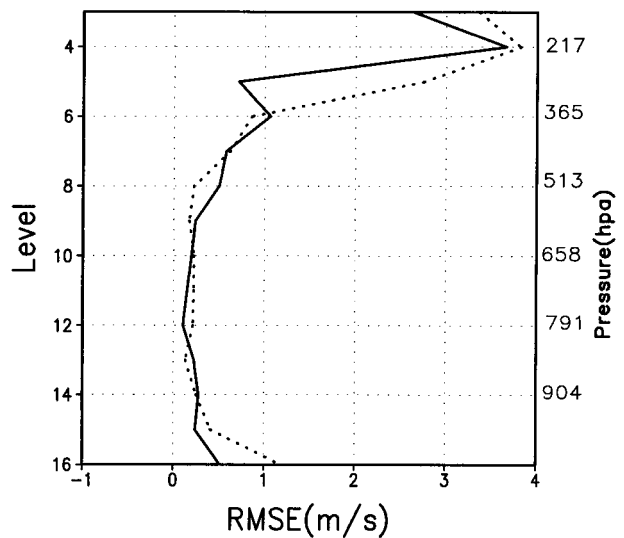


FIG. 9. Rmse of the estimated velocities for the diabatic experiment on a beta plane in a resting environment (E4). The solid and dashed lines are for the zonal and meridional components, respectively.

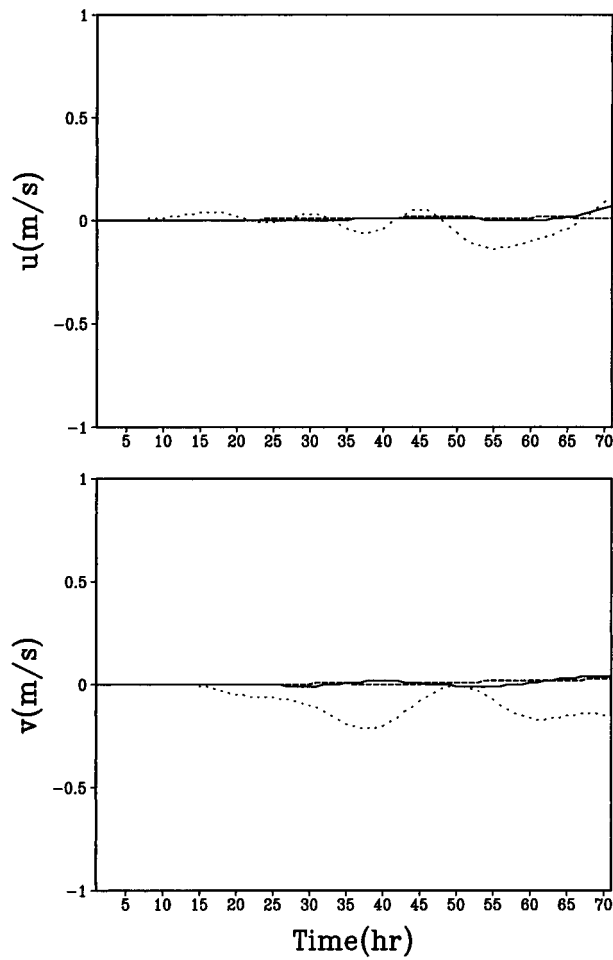


FIG. 10. The contributions of horizontal advection (solid), vertical advection (dashed), and diabatic heating (dotted) to the (top) zonal and (bottom) meridional velocities at level 11 in the diabatic experiment on an f plane with a resting environment (E2).

locities in Fig. 5 are caused by the influence of diabatic heating, because PV can be strongly influenced by small-scale effects.

Figure 11 further shows the contributions of the various processes to the beta drift in E4. In agreement with Wang and Holland (1996b), the TC circulation in this experiment is well coupled, and the vortices at lower and middle levels move at a similar speed. While the contributions from different physical processes vary with height, the estimated TC motion is almost invariant. At level 13 (850 mb), the vortex movement is primarily caused by the influence of horizontal PV advection, while at levels 9 (580 mb) and 11 (730 mb), both diabatic heating and the horizontal advection play an important role in the vortex motion. We will discuss how the diabatic heating can affect the TC motion in the next section. The above comparisons indicate that the proposed diagnostic approach is capable of detecting the contributions of physical processes to TC motion.

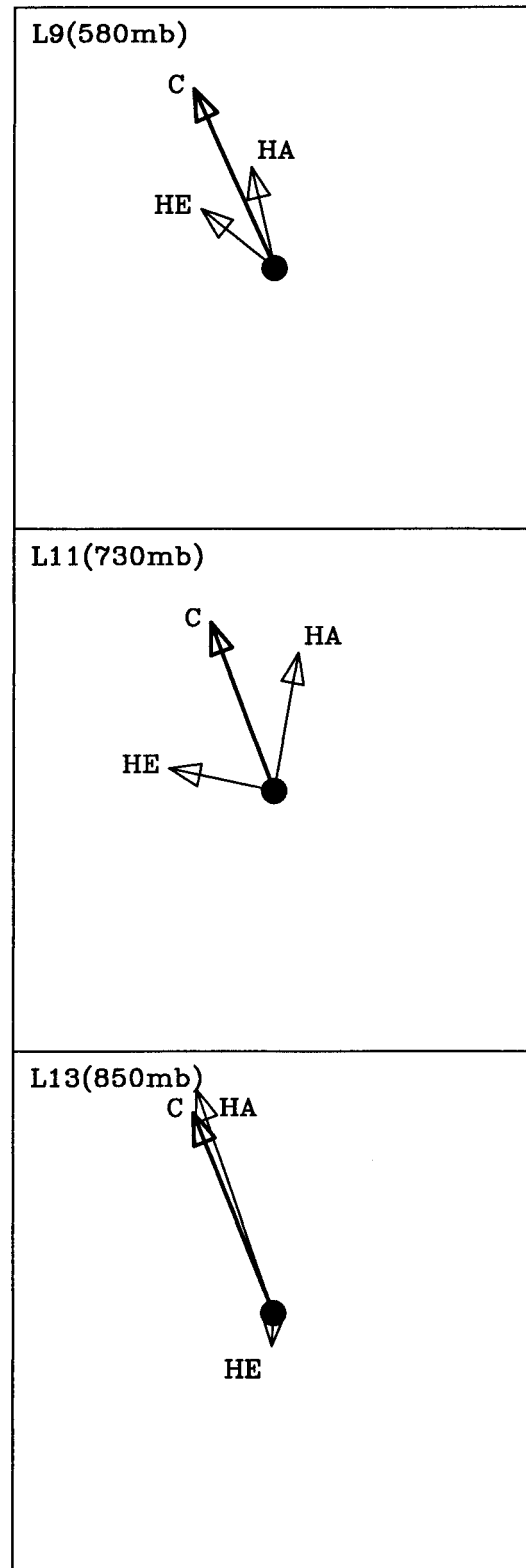


FIG. 11. Variations of the contributions (the maximum is 2.9 m s^{-1}) of horizontal advection (HA), vertical advection (VA), and diabatic heating (HE) at 36 h in the diabatic experiment on a beta plane with a resting environment (E4).

6. Summary

The ventilation flow (the axially asymmetric flow over the TC center) is one of the fundamental concepts for understanding propagation (or beta drift) of barotropic tropical cyclone. For a realistic baroclinic TC, especially in the presence of diabatic heating, both observations and numerical experiments have shown that the ventilation flow over the TC core exhibits considerable vertical variations, whereas the TC translates as an entity (Wu and Emanuel 1995a,b; Bender 1997; Wang and Holland 1996b). In this case, the concept of ventilation flow is of limited value. In order to understand the physical mechanisms involved in the baroclinic TC motion, a new perspective based on PV tendency for study of TC motion is advanced. A TC is treated as a PV anomaly compared with its environment. The vortex motion at a certain level is primarily determined by the wavenumber one component of the PV tendency, rather than the ventilation flow. We have demonstrated that the vortices at lower and middle levels tend to move to the region with maximum PV tendency.

We have shown that the azimuthal wavenumber one component of the PV tendency is primarily balanced by advection of axially symmetric PV by TC motion. This relation is valid at the lower and middle levels of a TC where the positive PV anomaly dominates. The relation lays a fundamental linkage between TC motion and the wavenumber one component of the PV tendency. The PV tendency is determined by various processes that govern PV evolution in a diabatic TC. Therefore, a linkage between various physical processes described in an Eulerian reference frame and the Lagrangian trajectory of the TC is established.

Based on this dynamical framework, a new diagnostic approach is proposed to estimate the vortex speed vector from the azimuthal wavenumber one component of the PV tendency. With idealized numerical experiments, in which the contributions of various physical processes are known, we demonstrate that the estimated TC motion is an excellent approximation to the vortex speed determined from the position of the vortex center. In the new approach, the fractional contributions of individual physical processes can be quantitatively estimated according to their contributions to the wavenumber one component of the PV tendency. Thus it is useful to investigate the physical mechanisms of TC motion and the associated vertical interaction. Note, however, that this approach can only be used when the symmetric PV component is dominant.

As shown in Eq. (5), diabatic heating can directly contribute to the wavenumber one component of the PV tendency. According to Hoskins et al. (1985), interior diabatic heating cannot change the mass-weighted total PV in a TC, but it does play a role in redistributing the PV by horizontal or vertical transports. The PV transport associated with diabatic heating is along the absolute vorticity vector (Raymond 1992). In E2, for example,

the PV transport associated with the symmetric heating can occur in the vertical due to the absence of the horizontal vorticity component. Due to symmetric heating, PV is removed from the upper levels and is deposited in the lower levels. It cannot contribute to the asymmetric PV tendency. In E4, however, the beta gyres lead to asymmetric wind fields in the boundary layer and, thus, in the fluxes of heat and moisture. The asymmetric fluxes can enhance the diabatic heating in the region with relatively high winds (Tuleya and Kurihara 1984). The PV transport associated with the asymmetric heating occurs in the vertical along the symmetric vorticity vector and contributes to the asymmetric PV tendency. In addition, the vertically differential beta effect can produce a relative horizontal vorticity component through the vertical shear of the asymmetric flow over the TC center. Thus PV transport associated with the symmetric heating can occur horizontally (Raymond 1992) and produce the asymmetric PV tendency. Therefore, diabatic heating can directly contribute to TC motion.

It should be pointed out that, although diabatic heating can directly contribute to the asymmetric PV tendency that leads to the vortex motion, the diabatic heating can also indirectly induce asymmetric wind fields that change the vortex motion. To assess the net effects of diabatic heating is beyond the scope of the present paper and will be discussed elsewhere.

Acknowledgments. We would like to thank Drs. L. Shapiro and K. Emanuel, and an anonymous reviewer for their careful review and valuable comments; Dr. Y. Wang for giving us his original code of the hurricane model; and Dr. T. A. Schroeder for his comments. This research is supported by the Marine Meteorology Program of the Office of Naval Research. BW is a member of the International Pacific Research Center (IPRC). IPRC is sponsored in part by the Frontier Research System for Global Change.

APPENDIX A

The Hurricane Model

a. Numerical details

The hurricane model designed by Wang (1998) is adopted in this study. The model consists of 201×201 grid points with a uniform spacing of 25 km and 16 vertical layers with relatively high resolution near the lower and upper boundaries. All variables are defined at the same grid point on the σ surface. The vertically dependent variables, such as the horizontal winds, temperature, and mixing ratio of water vapor, are defined in the middle of each layer, but the vertical velocity is staggered. As required by upper and lower boundary conditions, fluid particles do not cross the boundaries at $\sigma = 0$ and $\sigma = 1$. Sponge layers are used at the north and south boundaries and cyclonic boundary conditions are used in the zonal direction.

A two-time-level, explicit time-split scheme is used for time integration. The procedure consists of an advection stage of time step t_A , followed by N adjustment steps with a time step $t_L = t_A/N$. A full time step integration is completed with a physical process stage of time step t_A . The forward-in-time upstream advective scheme developed by Wang (1996) is adopted for the advection stage. This advection scheme has third-order accuracy for time-dependent and nonuniform flows with very small dissipation and phase errors and good shape-preserving properties. The adjustment stage is accomplished by a forward-backward scheme with the Coriolis force implicitly treated. An adjustment time step of $t_L = 60$ s is used and the number of adjustment steps per advection step is 2. For the horizontal differencing, a centered finite-difference scheme with fourth-order precision is used. The vertical difference scheme is identical to that used by Arakawa and Lamb (1977).

b. Model physics

The large-scale condensation is calculated explicitly with the method used by Leslie et al. (1985). Subgrid-scale cumulus convection is parameterized following Kuo (1974) with modifications suggested by Anthes (1977). To determine the model cloud profiles, the Newton-Raphson technique is used to solve the conservation law of moist static energy (appendix 2 of Wang 1995). The evaporation of precipitation is included in both large-scale and convective precipitation, following the method of Kessler (1969) since including evaporation has the effect of shrinking the area of low amounts of precipitation to more realistic values (Hess 1990).

A Newtonian cooling is added to the thermodynamic equation to include the radiation cooling, as used in the TC model by Rotunno and Emanuel (1987). The relaxation timescale for radiational cooling is taken to be a function of the radius from the vortex center. In the outer region 24 h is used, but it is gradually increased inward and reaches 96 h at the vortex center in order to avoid unrealistic cooling of the warm core of the model TCs.

Subgrid-scale horizontal diffusion of momentum, heat, and moisture is calculated in the manner given by Smagorinsky et al. (1965). The vertical eddy fluxes of momentum, heat, and moisture are parameterized by the method proposed by Louis (1979). The important feature of the scheme is the dependence of the diffusion coefficients on the static stability of the atmosphere and the vertical shears. Surface turbulent fluxes of momentum, and both sensible and latent heat, are calculated by the bulk aerodynamic method. The exchange coefficients are determined from the formula given by Kondo (1975) for neutral conditions and modified to be Richardson number dependent following Louis (1979).

c. Vortex initialization and experimental design

The tangential wind profile of the initial cyclonic vortex is

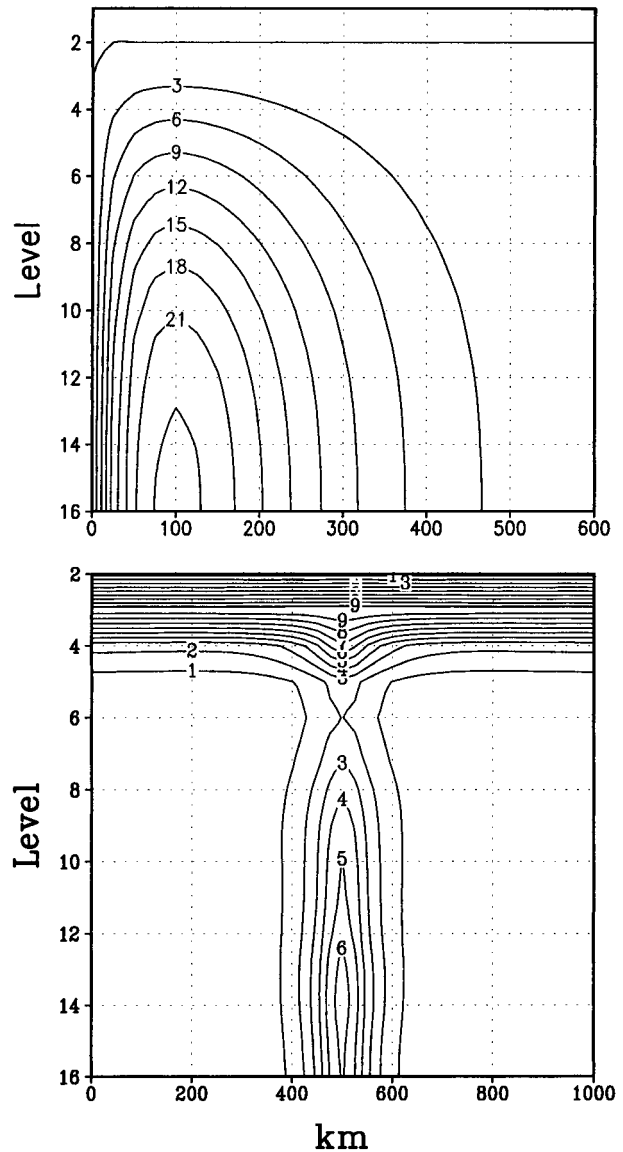


FIG. A1. The (top) initial azimuthal wind and (bottom) potential vorticity profiles with contours of 2 m s^{-1} for the wind and 1.0 PVU for potential vorticity.

$$V_T(r, \sigma) = V_m \left(\frac{r}{r_m} \right) \exp \left[1 - \left(\frac{r}{r_m} \right) \right] \sin \left[\frac{\pi (\sigma + 0.2)}{1.2} \right], \tag{A1}$$

where r denotes radial distance from the vortex center and V_m is the maximum azimuthal wind at the radius of r_m . At a given radial distance from the vortex center, the vortex has a maximum wind at the surface ($\sigma = 1$) and disappears at the top of the model ($\sigma = 0$).

The nonlinear balance equation is used to determine the initial mass field associated with the wind profile. An accurate and consistent numerical scheme is used to solve the inverse balance equation in multilevel primitive equation models using σ as the vertical coordinate

(Wang 1995). The new scheme incorporates the hydrostatic relation with the inverse balance equation so that approximations made in the previous studies (Sundqvist 1975) are eliminated.

Figure A1 shows the initial azimuthal wind and PV profiles. The undisturbed temperature profile is obtained from the clear-sky sounding in the western North Pacific (Gray et al. 1975), and $v_m = 25 \text{ m s}^{-1}$ at $r_m = 100 \text{ km}$. Notice that the initial cyclonic circulation is primarily confined within a radius of 600 km.

APPENDIX B

Potential Vorticity Tendency Equation

According to Hoskins et al. (1985), the PV in the pressure coordinates can be written as

$$P = -g(\mathbf{k}f + \nabla_p \times \mathbf{V}) \cdot \nabla_p \theta, \quad (\text{B1})$$

where

$$\mathbf{V} = u\mathbf{i} + v\mathbf{j}, \quad \text{and} \quad \nabla_p = \frac{\partial}{\partial x}\mathbf{i} + \frac{\partial}{\partial y}\mathbf{j} + \frac{\partial}{\partial p}\mathbf{k},$$

where \mathbf{i} , \mathbf{j} , and \mathbf{k} are the unit vectors in the pressure coordinates; u and v are the zonal and meridional wind components; and θ and g are the potential temperature and gravitational acceleration, respectively. If we define

$$\sigma = \frac{p}{p_s},$$

the definition of (B1) can be written in σ coordinate as

$$P = -\frac{g}{p_s} \left[(\zeta + f) \frac{\partial \theta}{\partial \sigma} + \frac{\partial u}{\partial \sigma} \frac{\partial \theta}{\partial y} - \frac{\partial v}{\partial \sigma} \frac{\partial \theta}{\partial x} \right], \quad (\text{B2})$$

where p , p_s , ζ , and f are the pressure, surface pressure, relative vorticity, and the Coriolis parameter, respectively.

Meanwhile, the governing equations in the σ coordinates are

$$\frac{du}{dt} - fv = -\frac{\partial \phi}{\partial x} - c_p \theta \frac{\partial \pi}{\partial x} + F_x, \quad (\text{B3})$$

$$\frac{dv}{dt} + fu = -\frac{\partial \phi}{\partial y} - c_p \theta \frac{\partial \pi}{\partial y} + F_y, \quad (\text{B4})$$

$$\frac{d \ln p_s}{dt} = -\left(\frac{\partial u}{\partial x} + \frac{\partial v}{\partial y} \right) - \frac{\partial \dot{\sigma}}{\partial \sigma}, \quad (\text{B5})$$

$$\frac{\partial \phi}{\partial \sigma} = -c_p \theta \frac{\partial \pi}{\partial \sigma}, \quad (\text{B6})$$

$$\frac{d\theta}{dt} = -\frac{Q}{c_p \pi}, \quad \text{and} \quad (\text{B7})$$

$$\pi = \left(\frac{p}{1000} \right)^{R/c_p}, \quad (\text{B8})$$

where ϕ , F_x , F_y , and Q are the geopotential height, friction component in the x and y directions, and diabatic heating rate, respectively. From Eqs. (B3) and (B4), the vorticity equation can be obtained as

$$\begin{aligned} \frac{d(\zeta + f)}{dt} = & -(\zeta + f) \left(\frac{\partial u}{\partial x} + \frac{\partial v}{\partial y} \right) + \frac{\partial \dot{\sigma}}{\partial y} \frac{\partial u}{\partial \sigma} - \frac{\partial \dot{\sigma}}{\partial x} \frac{\partial v}{\partial \sigma} \\ & - c_p \frac{\partial \theta}{\partial x} \frac{\partial \pi}{\partial y} + c_p \frac{\partial \theta}{\partial y} \frac{\partial \pi}{\partial x} + \frac{\partial F_y}{\partial x} - \frac{\partial F_x}{\partial y}. \end{aligned} \quad (\text{B9})$$

In addition, multiplying Eq. (B2) with p_s and differentiating with respect to time yields

$$\begin{aligned} \frac{d(Pp_s)}{dt} = & -g \frac{\partial \theta}{\partial \sigma} \frac{d}{dt} (f + \zeta) - g(f + \zeta) \frac{d}{dt} \left(\frac{\partial \theta}{\partial \sigma} \right) \\ & - g \frac{d}{dt} \left(\frac{\partial u}{\partial \sigma} \frac{\partial \zeta}{\partial y} - \frac{\partial v}{\partial \sigma} \frac{\partial \zeta}{\partial x} \right). \end{aligned} \quad (\text{B10})$$

Since

$$p_s \frac{dP}{dt} = \frac{d}{dt} (Pp_s) - P \frac{dp_s}{dt},$$

Eq. (B10) can be rewritten as

$$\begin{aligned} p_s \frac{dP}{dt} = & -g \frac{\partial \theta}{\partial \sigma} \frac{d}{dt} (f + \zeta) - g(f + \zeta) \frac{\partial}{\partial \sigma} \left(\frac{d\theta}{dt} \right) \\ & + g(f + \zeta) \left(\frac{\partial u}{\partial \sigma} \frac{\partial \theta}{\partial x} + \frac{\partial v}{\partial \sigma} \frac{\partial \theta}{\partial y} + \frac{\partial \dot{\sigma}}{\partial \sigma} \frac{\partial \theta}{\partial \sigma} \right) \\ & - g \frac{d}{dt} \left(\frac{\partial u}{\partial \sigma} \frac{\partial \theta}{\partial y} - \frac{\partial v}{\partial \sigma} \frac{\partial \theta}{\partial x} \right) - P \frac{dp_s}{dt}. \end{aligned} \quad (\text{B11})$$

Substituting Eqs. (B5), (B7), and (B9) into Eq. (B11) yields

$$\begin{aligned} \frac{\partial P}{\partial t} = & -u \frac{\partial P}{\partial x} - v \frac{\partial P}{\partial y} - \dot{\sigma} \frac{\partial P}{\partial \sigma} \\ & - \left(\frac{g}{p_s} \right) \left[\left(\frac{\partial F_y}{\partial x} - \frac{\partial F_x}{\partial y} \right) \frac{\partial \theta}{\partial \sigma} + \frac{\partial \theta}{\partial y} \frac{\partial F_x}{\partial \sigma} - \frac{\partial \theta}{\partial x} \frac{\partial F_y}{\partial \sigma} \right] \\ & + \left(\frac{g}{p_s} \right) \left[-(f + \zeta) \frac{\partial}{\partial \sigma} \left(\frac{Q}{c_p \pi} \right) - \frac{\partial u}{\partial \sigma} \frac{\partial}{\partial y} \left(\frac{Q}{c_p \pi} \right) \right. \\ & \left. + \frac{\partial v}{\partial \sigma} \frac{\partial}{\partial x} \left(\frac{Q}{c_p \pi} \right) \right] \quad \text{or} \end{aligned} \quad (\text{B12})$$

$$\frac{\partial P}{\partial t} = -\mathbf{V} \cdot \nabla P - \dot{\sigma} \frac{\partial P}{\partial \sigma} - \frac{g}{p_s} \nabla_3 \cdot \left(-\frac{Q}{C_p \pi} \mathbf{q} + \nabla \theta \times \mathbf{F} \right), \quad (\text{B13})$$

where $\dot{\sigma}$ is the vertical velocity in the σ coordinates, \mathbf{q} is the three-dimensional vorticity vector, and ∇_3 denotes the three-dimensional gradient operator.

REFERENCES

- Anthes, R. A., 1977: A cumulus parameterization scheme utilizing a one-dimensional cloud model. *Mon. Wea. Rev.*, **105**, 270–286.
- Arakawa, A., and V. R. Lamb, 1977: Computational design of the basic dynamical process of the UCLA general circulation model. *Methods Comput. Phys.*, **17**, 173–265.
- Bender, M. A., 1997: The effect of relative flow on the asymmetric structure in the interior of hurricanes. *J. Atmos. Sci.*, **54**, 703–724.
- Carr, L. E., and R. L. Elsberry, 1990: Observational evidence for predictions of tropical cyclone propagation relative to steering. *J. Atmos. Sci.*, **47**, 542–546.
- Chan, J. C.-L., 1984: An observational study of the physical processes responsible for tropical cyclone motion. *J. Atmos. Sci.*, **41**, 1036–1048.
- Davis, C. A., 1992: Piecewise potential vorticity inversion. *J. Atmos. Sci.*, **49**, 1397–1411.
- DeMaria, M., 1985: Tropical cyclone motion in a nondivergent barotropic model. *Mon. Wea. Rev.*, **113**, 1199–1209.
- Fiorino, M. J., and R. L. Elsberry, 1989: Some aspects of vortex structure related to tropical cyclone motion. *J. Atmos. Sci.*, **46**, 975–990.
- Gray, W. M., E. Ruprecht, and R. Phelps, 1975: Relative humidity in tropical weather systems. *Mon. Wea. Rev.*, **103**, 685–690.
- Hess, G. D., 1990: Numerical simulation of the August 1986 heavy rainfall event in the Sydney area. *J. Geophys. Res.*, **95** (D3), 2073–2082.
- Holland, G. J., 1983: Tropical cyclone motion: Environmental interaction plus a beta effect. *J. Atmos. Sci.*, **40**, 328–342.
- Hoskins, B. J., M. E. McIntyre, and A. W. Robertson, 1985: On the use and significance of isentropic potential vorticity maps. *Quart. J. Roy. Meteor. Soc.*, **111**, 877–946.
- Kessler, E., 1969: *On the Distribution and Continuity of Water Substance in Atmospheric Circulation*. Meteor. Mongr., No. 32, Amer. Meteor. Soc., 84 pp.
- Kondo, J., 1975: Air–sea bulk transfer coefficients in diabatic conditions. *Bound.-Layer Meteor.*, **9**, 91–112.
- Kuo, H. L., 1974: Further studies of the parameterization of the influence of cumulus convection on large-scale flow. *J. Atmos. Sci.*, **31**, 1232–1240.
- Leslie, B. M., G. A. Mills, L. W. Logan, D. J. Gauntlett, G. A. Kwilly, M. J. Manton, J. L. McGregor, and J. M. Sardie, 1985: A high resolution primitive equation NWP model for operations and research. *Aust. Meteor. Mag.*, **33**, 11–55.
- Li, X., and B. Wang, 1994: Barotropic dynamics of the beta gyres and beta drift. *J. Atmos. Sci.*, **51**, 746–756.
- , and —, 1996: Acceleration of the hurricane beta drift by shear strain rate of an environmental flow. *J. Atmos. Sci.*, **53**, 327–334.
- Louis, J. F., 1979: A parametric model of vertical eddy fluxes in the atmosphere. *Bound.-Layer Meteor.*, **17**, 182–202.
- Peng, M. S., and R. T. Williams, 1990: Dynamics of vortex asymmetries and their influence on vortex motion on a beta-plane. *J. Atmos. Sci.*, **47**, 1987–2003.
- Press, W. H., B. P. Flannery, S. T. Teukolsky, and W. T. Vetterling, 1986: *Numerical Recipes: The Art of Scientific Computing*. Cambridge University Press, 818 pp.
- Raymond, D. J., 1992: Nonlinear balance and potential-vorticity thinking at large Rossby number. *Quart. J. Roy. Meteor. Soc.*, **118**, 987–1015.
- Rotunno, R., and K. A. Emanuel, 1987: An air–sea interaction theory for tropical cyclones. Part II: Evolutionary study using a non-hydrostatic axisymmetric numerical model. *J. Atmos. Sci.*, **44**, 542–561.
- Shapiro, L. J., 1992: Hurricane vortex motion and evolution in a three-layer model. *J. Atmos. Sci.*, **49**, 140–153.
- , 1996: The motion of Hurricane Gloria: A potential vorticity diagnosis. *Mon. Wea. Rev.*, **124**, 2497–2508.
- , and M. T. Montgomery, 1993: A three-dimensional balance theory for rapidly rotating vortices. *J. Atmos. Sci.*, **50**, 3322–3335.
- , and J. L. Franklin, 1995: Potential vorticity in Hurricane Gloria. *Mon. Wea. Rev.*, **123**, 1465–1475.
- , and —, 1999: Potential vorticity asymmetries and tropical cyclone motion. *Mon. Wea. Rev.*, **127**, 124–131.
- Smagorinsky, J., S. Manabe, and J. L. Holloway Jr., 1965: Numerical results from a nine-level general circulation model of the atmosphere. *Mon. Wea. Rev.*, **93**, 727–768.
- Smith, R. K., 1991: An analytic theory of tropical-cyclone motion in a barotropic shear flow. *Quart. J. Roy. Meteor. Soc.*, **117**, 685–714.
- Sundqvist, H., 1975: Initialization for models using sigma as the vertical coordinate. *J. Appl. Meteor.*, **14**, 153–154.
- Tuleya, R. E., and Y. Kurihara, 1984: The formation of comma vortices in a tropical numerical simulation model. *Mon. Wea. Rev.*, **112**, 491–502.
- Ulrich, W., and R. K. Smith, 1991: A numerical study of tropical cyclone motion using a barotropic model. II: Motion in spatially-varying large-scale flows. *Quart. J. Roy. Meteor. Soc.*, **117**, 107–124.
- Wang, B., and X. Li, 1992: The beta drift of three-dimensional vortices: A numerical study. *Mon. Wea. Rev.*, **120**, 579–593.
- , and —, 1995: Propagation of a tropical cyclone in a meridional varying zonal flow: An energetics analysis. *J. Atmos. Sci.*, **52**, 1421–1433.
- , —, and L. Wu, 1997: Hurricane beta drift direction in horizontally sheared flows. *J. Atmos. Sci.*, **54**, 1462–1471.
- , R. L. Elsberry, Y. Wang, and L. Wu, 1998: Dynamics of tropical cyclone motion: A review. *Sci. Atmos. Sin.*, **22**, 1–12.
- Wang, Y., 1995: Baroclinic aspects of tropical cyclone motion. Ph.D. thesis, Monash University, 268 pp. [Available from Department of Meteorology, Monash University, Wellington Rd., Clayton, Vic 3168, Australia.]
- , 1996: On the forward-in-time upstream advection scheme for nonuniform and time-dependent flow. *Meteor. Atmos. Phys.*, **61**, 27–38.
- , 1998: On the bogusing of tropical cyclones in numerical models: The influence of vertical structure. *Meteor. Atmos. Phys.*, **65**, 153–170.
- , and G. J. Holland, 1996a: The beta drift of baroclinic vortices. Part I: Adiabatic vortices. *J. Atmos. Sci.*, **53**, 411–427.
- , and —, 1996b: The beta drift of baroclinic vortices. Part II: Diabatic vortices. *J. Atmos. Sci.*, **53**, 3737–3756.
- , and —, 1996c: Tropical cyclone motion and evolution in vertical shear. *J. Atmos. Sci.*, **53**, 3313–3332.
- Williams, R. T., and J. C.-L. Chan, 1994: Numerical studies of the beta effect in tropical cyclone motion. Part II: Zonal mean flow. *J. Atmos. Sci.*, **51**, 1065–1076.
- Willoughby, H. E., 1990: Temporal changes of the primary circulation in tropical cyclones. *J. Atmos. Sci.*, **47**, 242–264.
- , 1992: Linear motion of a shallow water barotropic vortex as an initial-value problem. *J. Atmos. Sci.*, **49**, 2015–2031.
- Wu, C.-C., and K. A. Emanuel, 1993: Interaction of a baroclinic vortex with background shear: Application to hurricane movement. *J. Atmos. Sci.*, **50**, 62–76.
- , and —, 1995a: Potential vorticity diagnostics of hurricane movement. Part I: A case study of Hurricane Bob (1991). *Mon. Wea. Rev.*, **123**, 69–92.
- , and —, 1995b: Potential vorticity diagnostics of hurricane movement. Part II: Tropical Storm Ana (1991) and Hurricane Andrew (1992). *Mon. Wea. Rev.*, **123**, 93–109.
- , and Y. Kurihara, 1996: A numerical study of the feedback mechanisms of hurricane–environment interaction on hurricane movement from the potential vorticity perspective. *J. Atmos. Sci.*, **53**, 2264–2282.